# Metal Hydride and Ligand Proton Transfer Mechanism for the Hydrogenation of Dimethyl Carbonate to Methanol Catalyzed by a Pincer Ruthenium Complex

**ARTICLE** *in* ACS CATALYSIS · APRIL 2012

Impact Factor: 9.31 · DOI: 10.1021/cs3000683



**1 AUTHOR:**

Xinzheng Yang
Chinese Academy of Sciences
**58** PUBLICATIONS **984** CITATIONS

SEE PROFILE

ACS Catalysis

Research Article

pubs.acs.org/acscatalysis

# Metal Hydride and Ligand Proton Transfer Mechanism for the Hydrogenation of Dimethyl Carbonate to Methanol Catalyzed by a Pincer Ruthenium Complex

Xinzheng Yang*

Molecular Graphics and Computation Facility, College of Chemistry, University of California, Berkeley, California 94720, United States

Supporting Information

**ABSTRACT:** The hydrogenation of dimethyl carbonate to methanol catalyzed by a PNN-ligated ruthenium complex (PNN)Ru(CO)(H) was studied computationally using the density functional theory at the range-separated and dispersion-corrected ωB97X-D functional level in conjunction with an all-electron 6-31++G(d,p) basis set (Stuttgart ECP28MWB basis set for Ru). A direct metal hydride and ligand proton transfer mechanism with three cascade catalytic cycles for the hydrogenation of dimethyl carbonate, methyl formate, and formaldehyde to methanol is proposed. The resting state in the catalytic reaction is the trans dihydride complex *trans*-(PNN)Ru(H)$_2$(CO). Calculation results indicate that the rate-determining step in the whole reaction is the formation of the second methanol molecule through simultaneous breaking of a C−OCH$_3$ bond and transferring a ligand methylene proton to the dissociated CH$_3$O$^-$ in the catalytic cycle for hydrogenation of methyl formate. The essential role of the noninnocent PNN pincer ligand is to split H$_2$ and assist methanol formation through the aromatization and dearomatization of the pyridine ring in the ligand. A new iron pincer complex, *trans*-(PNN)Fe(H)$_2$(CO), is proposed and evaluated as a promising low-cost and high efficiency catalyst for this reaction.

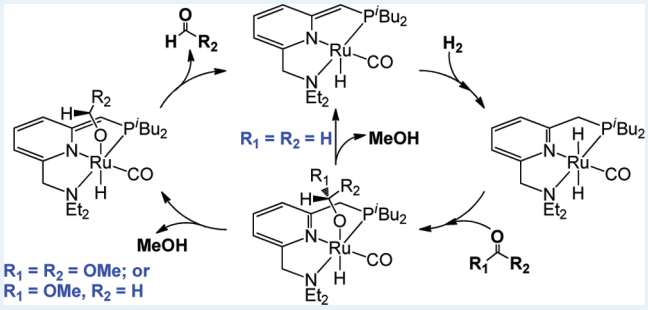


**KEYWORDS:** *hydrogenation, dimethyl carbonate, methyl formate, formaldehyde, methanol, ruthenium, iron, pincer ligand, homogeneous catalysis, catalytic mechanism, density functional theory*

## INTRODUCTION

Reutilization of carbon dioxide for the synthesis of valuable chemicals has attracted increasing attention not only because of the abundance, low-cost, and nontoxicity of $CO_2$ as a carbon source but also because of the strong desire of our society to protect the environment by reducing the $CO_2$ accumulation in the Earth's atmosphere.[1−3] As a key link in $CO_2$ conversion and utilization, the hydrogenation of small organic carbonyl compounds readily formed from $CO_2$ or CO, such as ketones, carbonates, carbamates, and formates, is significant conceptually in synthetic chemistry and practically in pharmaceutical and fine chemical industries. In addition, some small organic carbonyl compounds, like formic acid, aldehydes, and ketones, have potential applications in hydrogen storage and energy recovery.[4−6] For the purpose of developing high efficiency and low-cost catalysts for the reutilization of $CO_2$, significant progress has been achieved in iron based hydrogenation of $CO_2$ for the formation of formic acid and hydrogenation of ketones for the formation of alcohols.[7−10] Although methanol can be produced industrially through hydrogenation of CO and $CO_2$, the current procedure requires rather high pressure and temperature (250−300 °C). Very recently, Milstein and co-workers[11,12] developed an efficient catalytic system for the hydrogenation of organic carbonates to alcohols, and carbamates to alcohols and amines using ruthenium PNN pincer complexes (PNN)Ru(CO)(H) (Scheme 1) as the catalysts. In their experiments, dimethyl carbonate and methyl formate can be selectively hydrogenated to methanol under relatively mild conditions (10−60 atm $H_2$, 110−145 °C). Later on, Sanford and co-workers[13] also reported the hydrogenation of methyl formate to methanol catalyzed by the same (PNN)Ru(CO)(H) complexes in their study of cascade catalysis for the homogeneous hydrogenation of $CO_2$ to

**Scheme 1. Catalytic Hydrogenation of Dimethyl Carbonate to Methanol**

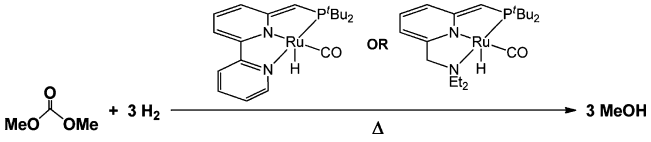


Received: January 29, 2012
Revised: March 12, 2012
Published: April 18, 2012

  

**Scheme 2. Predicted Catalytic Cycle for the Hydrogenation of Dimethyl Carbonate and the Formation of Methyl Formate and the First Methanol Molecule**

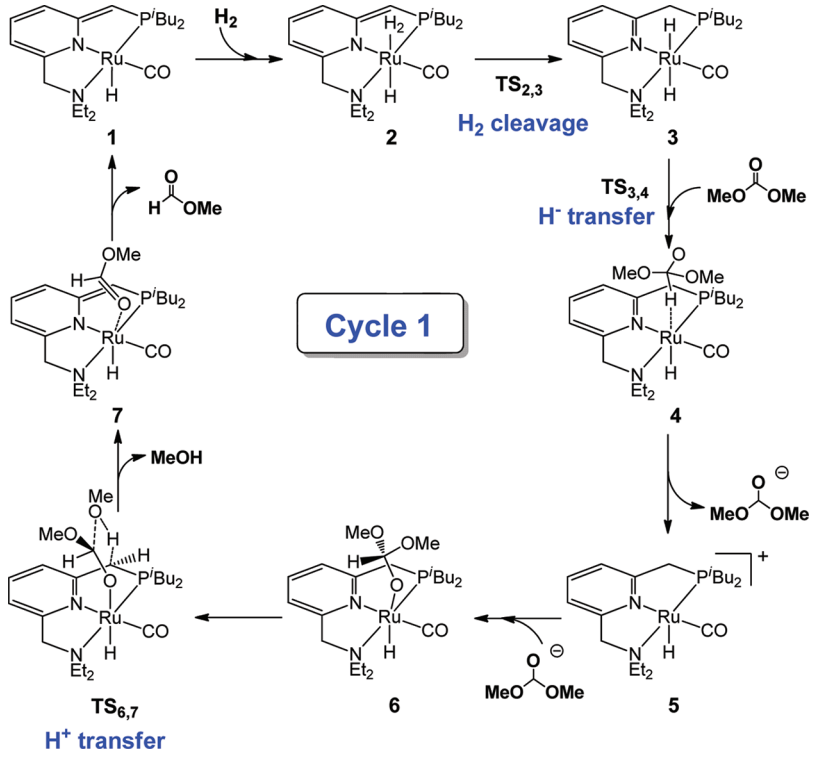


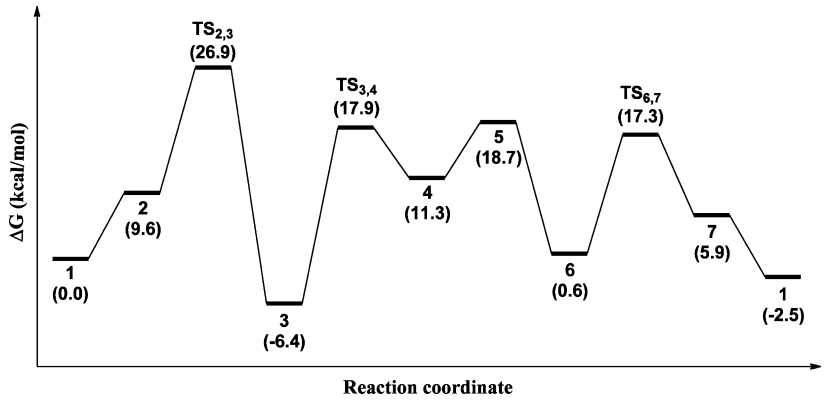


**Figure 1.** Calculated relative free energies in the catalytic cycle for the hydrogenation of dimethyl carbonate and the formation of the first methanol molecule.

methanol. The discovery of the above catalytic reactions has established a route for the low-cost conversion of CO and $CO_2$ to methanol under mild condition. Further improvement of current catalysts and the design of new metal complexes with higher efficiency and reduced cost for the hydrogenation of small organic carbonyl compounds rely on a deep understanding of related reaction mechanisms. Although a postulated catalytic cycle that involves metal−ligand cooperation by aromatization-dearomatization of the heteroaromatic pincer ligand and hydride transfer to the carbonyl group was proposed by Milstein and co-workers, a detailed reaction mechanism, especially the information of the rate-determining step of such reaction, is still unknown.

In this Article, I report for the first time the computational investigations into the hydrogenation of dimethyl carbonate to methanol catalyzed by (PNN)Ru(CO)(H) (**1**, PNN = 2-(di-*tert*-butylphosphinomethyl)-6-diethylaminomethyl)pyridine) using the density functional theory. A direct metal hydride and ligand proton transfer mechanism with three cascade catalytic cycles for the hydrogenation of dimethyl carbonate, methyl formate, and formaldehyde to methanol is proposed based on the calculation results. A detailed energy profile and transition state structures were obtained. The essential role of non-innocent pincer ligand in the rate-determining $H_2$ cleavage, C−O bond breaking and O−H bond formation processes was revealed and analyzed in depth. Furthermore, a new iron pincer complex, *trans*-(PNN)Fe(H)$_2$(CO), is proposed and evaluated as a promising low-cost and high efficiency catalyst for this reaction.

## RESULTS AND DISCUSSION

**Hydrogenation of Dimethyl Carbonate.** The catalytic cycle for the hydrogenation of dimethyl carbonate and the formation of methyl formate and the first methanol molecule


dx.doi.org/10.1021/cs3000683 | ACS Catal. 2012, 2, 964−970

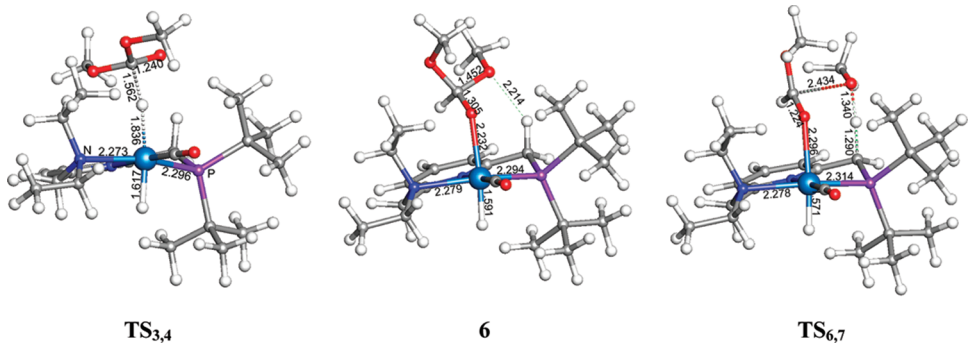


**Figure 2.** Optimized structures of $TS_{3,4}$ (867*i* $cm^{-1}$), **6** and $TS_{6,7}$ (1025*i* $cm^{-1}$). Bond lengths are in angstroms.

**Scheme 3. Predicted Catalytic Cycle for the Hydrogenation of Methyl Formate and the Formation of the Second Methanol Molecule**

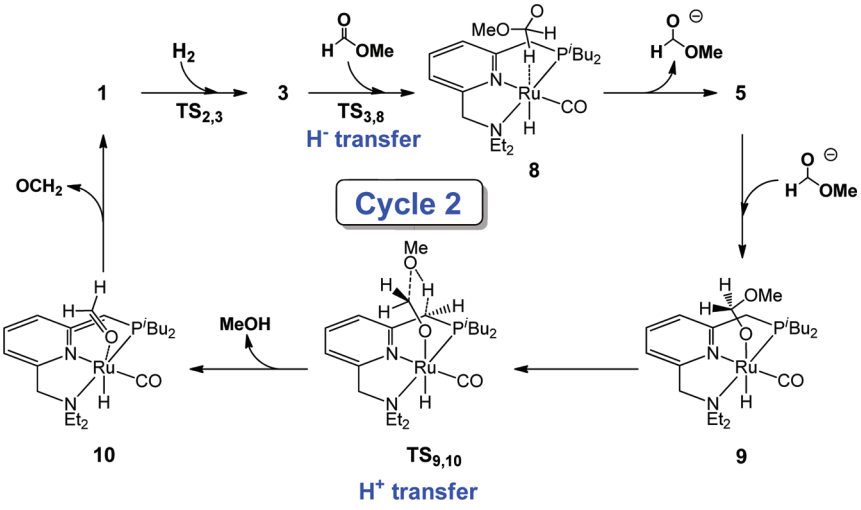


(Cycle 1) is shown in Scheme 2. The corresponding free energy profile is shown in Figure 1. The optimized structures of two important transition states and a stable intermediate for metal hydride transfer and C−O bond cleavage are shown in Figure 2.

At the beginning of the reaction, a dihydrogen molecule fills the vacant position in **1** and forms an unstable intermediate (PNN)Ru($H_2$)(CO)(H) (**2**). The $H_2$ in **2** can easily be split by Ru and the unsaturated carbon in the phosphorus side arm of the pincer ligand. A stable *trans*-dihydride complex *trans*-(PNP)Ru(H)$_2$(CO) (**3**) is therefore formed through $TS_{2,3}$ with a free energy barrier of 26.9 kcal/mol (**1** → $TS_{2,3}$) for $H_2$ cleavage. When a dimethyl carbonate molecule approaches **3**, it takes a hydride directly from Ru to its unsaturated carbon and forms an anionic ligand $(MeO)_2CHO^-$ through transition state $TS_{3,4}$ (Figure 2) with a free energy barrier of 24.3 kcal/mol (**3** → $TS_{3,4}$). An unstable hydrido alkoxo complex **4** is therefore formed. The dissociation of $(MeO)_2CHO^-$ from **4** for the formation of monocation **5** is an only 7.4 kcal/mol uphill step in the tetrahydrofuran (THF) solvent. Such low barrier indicates that the transformation of **4** to its more stable isomer **6** (Figure 2) with the formation of a Ru−O bond of 2.232 Å is very fast. All attempts to locate a transition state for direct migratory insertion of the carbonyl compound into the metal-hydride failed.

Once **6** is formed, a transition state $TS_{6,7}$ (Figure 2) simultaneously breaks a C−$OCH_3$ bond in the $(MeO)_2CHO$ ligand and transfers a proton from the methylene in the phosphorus side arm of the PNN ligand to the dissociated $MeO^-$ group. The first methanol molecule is therefore formed and released from the metal complex. The dissociation of MeOH leaves a methyl formate molecule bonding to Ru with a Ru−O distance of 2.330 Å in **7**. The dissociation the methyl formate molecule from **7** for the regeneration of **1** is an 8.4 kcal/mol downhill step in free energy.

**Hydrogenation of Methyl Formate.** The catalytic cycle for the hydrogenation of methyl formate for the formation of formaldehyde and the second methanol molecule (Cycle 2) is shown in Scheme 3. The corresponding free energy profile is shown in Figure 3. The optimized structures of two key

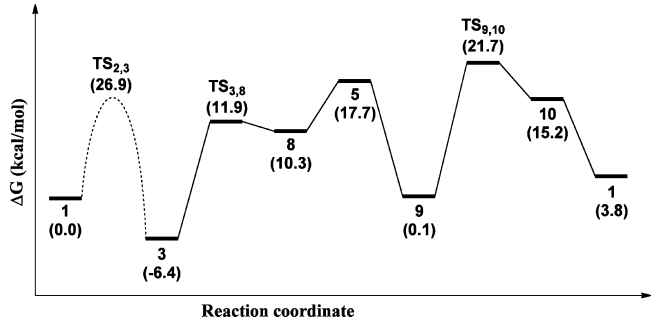


**Figure 3.** Calculated relative free energies in the catalytic cycle for the hydrogenation of methyl formate and the formation of formaldehyde and the second methanol molecule.


dx.doi.org/10.1021/cs3000683 | ACS Catal. 2012, 2, 964−970

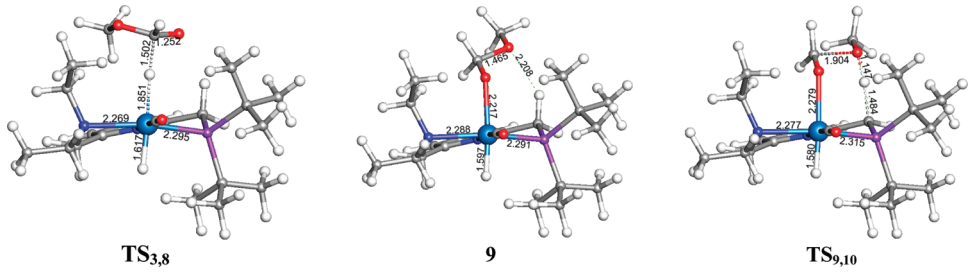


**Figure 4.** Optimized structures of $TS_{3,8}$ (811*i* $cm^{-1}$), **9**, and $TS_{9,10}$ (960*i* $cm^{-1}$). Bond lengths are in angstroms.

**Scheme 4. Predicted Catalytic Cycle for the Hydrogenation of Formaldehyde and the Formation of the Third Methanol Molecule**

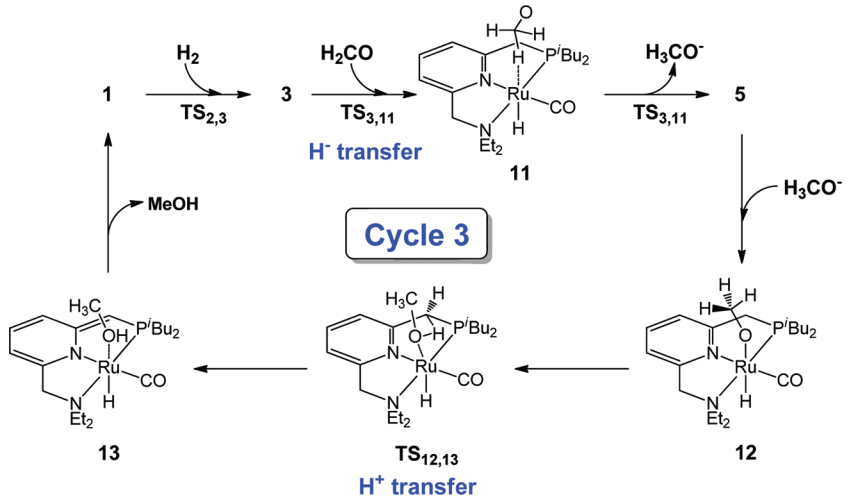


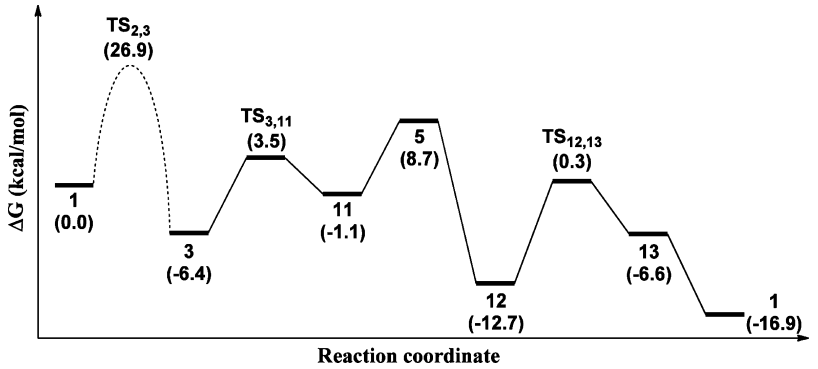


**Figure 5.** Calculated relative free energies in the catalytic cycle for the hydrogenation of formaldehyde and the formation of the third methanol molecule.

transition states and a stable intermediate for metal hydride transfer and C−O bond cleavage are shown in Figure 4.

Similar to hydrogenation of dimethyl carbonate, Cycle 2 also begins with $H_2$ cleavage and the formation of *trans* dihydride complex **3** through $TS_{2,3}$. Then a methyl formate molecule approaches **3**, transfers a hydride from Ru to its unsaturated carbon and forms an anionic ligand $MeOCH_2O^-$ through transition state $TS_{3,8}$ (Figure 4) with a free energy barrier of 18.4 kcal/mol. The unstable hydrido alkoxo complex **8** can easily transform to a more stable isomer **9** (Figure 4) through the dissociation and reassociation of $MeOCH_2O^-$. The Ru−O distance in **9** is 2.217 Å, slightly shorter than the Ru−O distance in **6**. Then a transition state $TS_{9,10}$ (Figure 4) simultaneously breaks the C−$OCH_3$ bond in $MeOCH_2O^-$ and transfers a proton from the phosphorus side methylene to the dissociated $MeO^-$ group. A methanol molecule is therefore formed and released from the metal complex. The dissociation of MeOH leaves a formaldehyde molecule in the unstable intermediate **10** with a Ru−O distance of 2.293 Å, which is about 0.07 and 0.06 Å longer than the Ru−O distances in **9** and **6**, respectively. The dissociation of $OCH_2$ from **10** is an 11.4 kcal/mol downhill step. The rate-determining step in this catalytic cycle is $TS_{9,10}$ with a total free energy barrier of 28.1 kcal/mol (**3** → $TS_{9,10}$).

**Hydrogenation of Formaldehyde.** The catalytic cycle for the hydrogenation of formaldehyde and the formation of the third methanol molecule (Cycle 3) is shown in Scheme 4. The free energy profile is shown in Figure 5. The optimized structures of two transition states and a stable intermediate for


dx.doi.org/10.1021/cs3000683 | *ACS Catal.* 2012, 2, 964−970

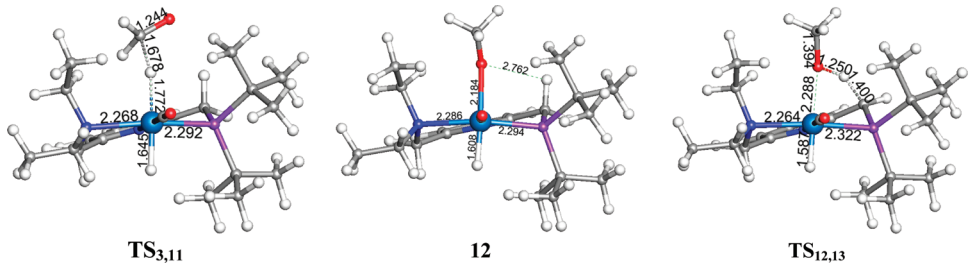


$TS_{3,11}$ 12 $TS_{12,13}$

**Figure 6.** Optimized structures of $TS_{3,11}$ (459*i* $cm^{-1}$), **12**, and $TS_{12,13}$ (1445*i* $cm^{-1}$) in the hydrogenation of formaldehyde and the formation of the third methanol molecule. Bond lengths are in angstroms.

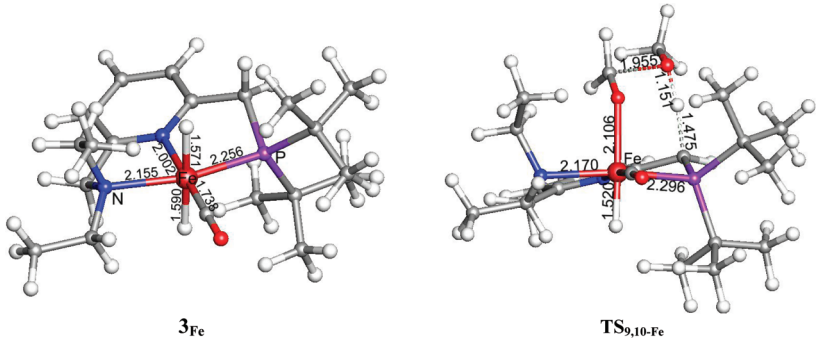


$3_{Fe}$ $TS_{9,10\text{-}Fe}$

**Figure 7.** Optimized structures of $3_{Fe}$ and $TS_{9,10\text{-}Fe}$ (982*i* $cm^{-1}$). Bond lengths are in angstroms.

metal hydride transfer to formaldehyde and methylene proton transfer to $CH_3O$ are shown in Figure 6.

Similar to hydrogenation of dimethyl carbonate and dimethyl formate, Cycle 3 also begins with formation of **3** through direct $H_2$ cleavage ($TS_{2,3}$). Then a hydride is transferred directly from Ru to the unsaturated carbon atom in $CH_2O$ when a formaldehyde molecule approaches **3**. The newly formed unstable intermediate **11** can easily transform to a much more stable isomer **12** (Figure 6) through the dissociation and reassociation of $CH_3O^-$. The Ru−O bond in **12** is 2.184 Å, which indicates a stronger interaction between Ru and the methoxy group. The following transition state $TS_{12,13}$ (Figure 6) transfers a proton from the phosphorus side methylene to the oxygen in the methoxy group and forms the third methanol molecule directly. The free energy barriers of the hydride transfer (**3** → $TS_{3,11}$) and proton transfer (**12** → $TS_{12,13}$) steps in this catalytic cycle are only 8.9 and 13.0 kcal/mol, respectively. Such low barriers indicate that the formation of methanol from formaldehyde is very fast. The dissociation of methanol from **13** for the regeneration of **1** is a 10.4 kcal/mol downhill step. By comparing all energy barriers in the above three catalytic cycles, we can conclude that the formation of the second methanol molecule in Cycle 2 is the rate-determining step with a total free energy barrier of 28.1 kcal/mol (**3** → $TS_{9,10}$) in the whole reaction. Such large energy barrier explains the observed slow conversion rate of the hydrogenation of methyl formate to methanol (48 h for a turnover number of 1155 at 110 °C).[11]

**Design of New Catalyst.** In their experimental study, Milstein and co-workers also observed the hydrogenation of dimethyl carbonate catalyzed by a bipyridine-based PNN pincer ruthenium complex, whose catalytic efficiency is very close to **1**. The improvement of current catalyst and further design of new catalysts with higher efficiency relies on a deep understanding of the effect of both ligands and transition metals in the rate-determining step. Inspired by the structures of recently reported pincer iron(II) complexes, *trans*-(PNP)Fe(H)$_2$CO and (PNN)FeCl$_2$,[8−10,14] a new trans dihydride iron PNN pincer complex, *trans*-(PNN)Fe(H)$_2$(CO) ($3_{Fe}$), is constructed by replacing the ruthenium atom in **3** with an iron atom. The optimized structure of stable Fe(II) complex $3_{Fe}$ is shown in Figure 7.

To evaluate the potential of $3_{Fe}$ as a low-cost catalyst for the hydrogenation of dimethyl carbonate to methanol, the transition state for the cleavage of the C−$OCH_3$ bond in methyl formate (Cycle 2) by $3_{Fe}$ was calculated using the same method. Such transition state was selected for comparison because $TS_{9,10}$ is the rate-determining step in the reaction catalyzed by **3**. A new transition state, $TS_{9,10\text{-}Fe}$, was located with a C···$OCH_3$ distance of 1.955 Å, which is slightly longer than that in $TS_{9,10}$. The optimized structure of $TS_{9,10\text{-}Fe}$ are shown in Figure 7. Compared to the 28.1 kcal/mol total energy barrier (**3** → $TS_{9,10}$) of the ruthenium complex, $TS_{9,10\text{-}Fe}$ is only 24.7 kcal/mol higher than $3_{Fe}$ in free energy. This means the newly constructed PNN pincer iron complex significantly lowers the free energy barrier of the rate-determining step by 3.4 kcal/mol. Therefore, $3_{Fe}$ is a very promising low-cost and high efficiency catalyst for the hydrogenation of dimethyl carbonate to methanol.

## CONCLUSIONS

In summary, the hydrogenation of dimethyl carbonate to methanol catalyzed by the ruthenium PNN pincer complex (PNN)Ru(CO)(H) was studied using the density functional theory. A direct reduction mechanism, which features with direct hydride transfer from the Ru center to the unsaturated carbon for the formation of hydrido alkoxo complexes and C−O bond cleavage by the noninnocent pincer ligand, was proposed based on the computational study. There are three cascade catalytic cycles for the splitting of three $H_2$ and the generation of three methanol molecules by the hydrogenation of dimethyl carbonate, methyl formate, and formaldehyde. The


dx.doi.org/10.1021/cs3000683 | *ACS Catal.* 2012, 2, 964−970

rate-determining step in the whole catalytic reaction is the simultaneous breaking of the C−O bond in $MeOCH_2O^-$ and transferring of a methylene proton to the dissociated $MeO^-$ group in Cycle 2. The calculated total free energy barrier of 28.1 kcal/mol (**3** → $\mathbf{TS}_{9,10}$) matches well with the observed turnover frequency of 24 $h^{-1}$ at 110 °C.[11] The essential role of the noninnocent PNN pincer ligand is to assist the splitting of $H_2$ and the formation of methanol molecules through the aromatization and dearomatization of the pyridine ring in the ligand. Such unusual participation of unsaturated ligand carbon atoms has also been predicted experimentally and theoretically in the catalytic water splitting and $H_2$ formation by the same (PNN)Ru(CO)(H) complex.[15−17]

The newly proposed mechanism also suggests that modification of the metal center and the noninnocent pincer ligand may lower the energy barrier of the rate-determining C−O bond cleavage step, provide a more favorable geometry for methylene proton transfer, and increase the overall efficiency for alcohol production from organic carbonates and formates. To further understand the effect of metal atoms in the catalytic reaction, a new trans dihydride iron PNN pincer complex, $\mathbf{3}_{Fe}$, is constructed computationally by replacing the ruthenium atom in **3** with an iron atom. The optimized transition state $\mathbf{TS}_{9,10\text{-}Fe}$ is only 24.7 kcal/mol higher than $\mathbf{3}_{Fe}$ in free energy. Such low barrier indicates that $\mathbf{3}_{Fe}$ is a very promising low-cost and high efficiency catalyst for the hydrogenation of dimethyl carbonate. Further computational studies of $\mathbf{3}_{Fe}$ as a catalyst for the reduction of $CO_2$ and small organic carbonyl compounds are underway.

## COMPUTATIONAL DETAILS

All DFT calculations were performed using the Gaussian 09 suite of ab initio programs[18] at the range-separated and dispersion-corrected hybrid functional ωB97X-D[19] level of theory. Experimental *tert*-butyl and isopropyl groups were employed without any simplification in the computational study. Stuttgart relativistic effective core potential (ECP) basis sets, ECP28MWB and ECP10MDF (8s7p6d2f1g → 6s5p3d2f1g),[20,21] were used for Ru and Fe, respectively. The all-electron 6-31++G(d,p) basis set[22−24] was used for all atoms in the dimethyl carbonate, atoms bonding to Ru (metal hydride, N, and P), and atoms in two methylene groups in the PNN ligand. The 6-31G(d,p) basis set was used for all other atoms which are far from the metal center. Such basis sets (for example, 762 basis functions for **4**) are sufficient for accurate DFT calculations. The ωB97X-D functional was selected for this study because it has both long-range exchange and empirical dispersion corrections, which are very important for the modeling of processes with weak interactions and localized anionic or strongly electron donating sites.[25,26] The importance of noncovalent attractive interactions in ruthenium complexes was recently studied by Truhlar and co-workers.[27] The ωB97X-D functional was recently evaluated as one of the most encouraging functionals in the study of the structure parameters in ruthenium complexes[28] and the kinetic barriers in an ethylene addition to nickel bis(dithiolene) reaction.[29,30]

All structures studied in this paper were fully optimized with solvent corrections using the integral equation formalism polarizable continuum model (IEFPCM)[31] with radii and cavity-dispersion-solvent-structure terms in Truhlar and co-workers' SMD solvation model[32] for THF ($\varepsilon$ = 7.4257). An ultrafine integration grid (99,590) was used for numerical integrations. The ground states of intermediates and transition states were confirmed as singlets through comparison with the optimized high-spin analogues. Thermal corrections were calculated within the harmonic potential approximation on optimized structures under $T$ = 298.15 K and 1 atm pressure. Unless otherwise noted, the energies reported in the text are solvent corrected free energies. Calculating the harmonic vibrational frequencies for optimized structures and noting the number of imaginary frequencies (IFs) confirmed the nature of all intermediates (no IF) and transition state structures (only one IF). The latter were also confirmed to connect reactants and products by intrinsic reaction coordinate (IRC) calculations. The 3D molecular structure figures displayed in this paper were drawn by using the JIMP2 molecular visualizing and manipulating program.[33]

## ASSOCIATED CONTENT

### Supporting Information

Absolute free energies and atomic coordinates of all optimized structures. This material is available free of charge via the Internet at http://pubs.acs.org.

## AUTHOR INFORMATION

### Corresponding Author

*E-mail: yangxz@berkeley.edu, yangxinzheng@gmail.com.

### Funding

This work was supported by the Molecular Graphics and Computation Facility (Dr. Kathleen A. Durkin, Director) in the College of Chemistry at University of California, Berkeley, and by the U.S. National Science Foundation (CHE-0840505) for the computational devices.

### Notes

The authors declare no competing financial interest.

## REFERENCES

(1) Jessop, P. G.; Joó, F.; Tai, C.-C. *Coord. Chem. Rev.* **2004**, *248*, 2425.
(2) Aresta, M., Ed.; *Carbon Dioxide as a Chemical Feedstock*; Wiley-VCH: Weinheim, Germany, 2010.
(3) Bakac, A., Ed.; *Physical Inorganic Chemistry*; John Wiley & Sons: Hoboken, NJ, 2010; pp 247−279.
(4) Ott, S. *Science* **2011**, *333*, 1714.
(5) Boddien, A.; Mellmann, D.; Gärtner, F.; Jackstell, R.; Junge, H.; Dyson, P. J.; Laurenczy, G.; Ludwig, R.; Beller, M. *Science* **2011**, *333*, 1733.
(6) Angelici, R. J. *ACS Catal.* **2011**, *1*, 772.
(7) Langer, R.; Leitus, G.; Ben-David, Y.; Milstein, D. *Angew. Chem., Int. Ed.* **2011**, *50*, 2120.
(8) Langer, R.; Diskin-Posner, Y.; Leitus, G.; Shimon, L. J. W.; Ben-David, Y.; Milstein, D. *Angew. Chem., Int. Ed.* **2011**, *50*, 9948.
(9) Yang, X. *ACS Catal.* **2011**, *1*, 849.
(10) Yang, X. *Inorg. Chem.* **2011**, *50*, 12836.
(11) Balaraman, E.; Gunanathan, C.; Zhang, J.; Shimon, L. J.; Milstein, D. *Nat. Chem.* **2011**, *3*, 609.
(12) Dixneuf, P. H. *Nat. Chem.* **2011**, *3*, 578.
(13) Sanford, M. S.; Huff, C. A. *J. Am. Chem. Soc.* **2011**, *133*, 18122.
(14) Zhang, J.; Gandelman, M.; Herrman, D.; Leitus, G.; Shimon, L. J. W.; Ben-David, Y.; Milstein, D. *Inorg. Chim. Acta* **2006**, *359*, 1955.
(15) Kohl, S. W.; Weiner, L.; Schwartsburd, L.; Konstantinovski, L.; Shimon, L. J. W.; Ben-David, Y.; Iron, M. A.; Milstein, D. *Science* **2009**, *324*, 74.
(16) Yang, X.; Hall, M. B. *J. Am. Chem. Soc.* **2010**, *132*, 120.
(17) Li, J.; Shiota, Y.; Yoshizawa, K. *J. Am. Chem. Soc.* **2009**, *131*, 13584.
(18) Frisch, M. J.; Trucks, G. W.; Schlegel, H. B.; Scuseria, G. E.; Robb, M. A.; Cheeseman, J. R.; Scalmani, G.; Barone, V.; Mennucci,

B.; Petersson, G. A.; Nakatsuji, H.; Caricato, M.; Li, X.; Hratchian, H. P.; Izmaylov, A. F.; Bloino, J.; Zheng, G.; Sonnenberg, J. L.; Hada, M.; Ehara, M.; Toyota, K.; Fukuda, R.; Hasegawa, J.; Ishida, M.; Nakajima, T.; Honda, Y.; Kitao, O.; Nakai, H.; Vreven, T.; Montgomery, Jr., J. A.; Peralta, J. E.; Ogliaro, F.; Bearpark, M.; Heyd, J. J.; Brothers, E.; Kudin, K. N.; Staroverov, V. N.; Kobayashi, R.; Normand, J.; Raghavachari, K.; Rendell, A.; Burant, J. C.; Iyengar, S. S.; Tomasi, J.; Cossi, M.; Rega, N.; Millam, N. J.; Klene, M.; Knox, J. E.; Cross, J. B.; Bakken, V.; Adamo, C.; Jaramillo, J.; Gomperts, R.; Stratmann, R. E.; Yazyev, O.; Austin, A. J.; Cammi, R.; Pomelli, C.; Ochterski, J. W.; Martin, R. L.; Morokuma, K.; Zakrzewski, V. G.; Voth, G. A.; Salvador, P.; Dannenberg, J. J.; Dapprich, S.; Daniels, A. D.; Farkas, Ö.; Foresman, J. B.; Ortiz, J. V.; Cioslowski, J.; Fox, D. J. *Gaussian 09*, revision B.01; Gaussian, Inc.: Wallingford, CT, 2010.

(19) Chai, J. -D.; Head-Gordon, M. *Phys. Chem. Chem. Phys.* **2008**, *10*, 6615.

(20) Martin, J. M.; Sundermann, A. *J. Chem. Phys.* **2001**, *114*, 3408.

(21) Andrae, D.; Haeussermann, U.; Dolg, M.; Stoll, H.; Preuss, H. *Theor. Chim. Acta* **1990**, *77*, 123.

(22) Hehre, W. J.; Ditchfield, R.; Pople, J. A. *J. Chem. Phys.* **1972**, *56*, 2257.

(23) Hariharan, P. C.; Pople, J. A. *Theor. Chim Acta* **1973**, *28*, 213.

(24) Krishnan, R.; Binkley, J. S.; Seeger, R.; Pople, J. A. *J. Chem. Phys.* **1980**, *72*, 650.

(25) Jensen, F. *J. Chem. Theory Comput.* **2010**, *6*, 2726.

(26) Thanthiriwatte, K. S.; Hohenstein, E. G.; Burns, L. A.; Sherrill, C. D. *J. Chem. Theory Comput.* **2011**, *7*, 88.

(27) Zhao, Y.; Truhlar, D. G. *Org. Lett.* **2007**, *9*, 1967.

(28) Kulkarni, A. D.; Truhlar, D. G. *J. Chem. Theory Comput.* **2011**, *7*, 2325.

(29) Dang, L.; Yang, X.; Brothers, E. N.; Hall, M. B. *J. Phys. Chem. A* **2012**, *116*, 476.

(30) Dang, L.; Shibl, M. F.; Yang, X.; Alak, A.; Harrison, D. J.; Fekl, U.; Brothers, E. N.; Hall, M. B. *J. Am. Chem. Soc.* **2012**, *134* (10), 4481.

(31) Tomasi, J.; Mennucci, B.; Cammi, R. *Chem. Rev.* **2005**, *105*, 2999.

(32) Marenich, A. V.; Cramer, C. J.; Truhlar, D. G. *J. Phys. Chem. B* **2009**, *113*, 6378.

(33) Manson, J.; Webster, C. E.; Hall, M. B. *JIMP2, version 0.091, a free program for visualizing and manipulating molecules*; Texas A&M University: College Station, TX, 2006.